九州工業大学学術機関リポジトリ

Kyutacar
Kyushu Institute of Technology Academic Repository

First-Principles Study on Hydrogen Diffusivity in BCC, FCC, and HCP Iron

First-principles study on hydrogen diffusivity in BCC, FCC, and HCP iron

K. Hirata[1], S. Iikubo[1*], M. Koyama[2], K. Tsuzaki[2], and H. Ohtani[3]

[1]Graduate School of Life Science and Systems Engineering, Kyushu Institute of Technology, Kitakyushu 808-0196, Japan

[2]Department of Mechanical Engineering, Kyushu University, 744 Motooka, Nishi-ku, Fukuoka 819-0395, Japan

[3]Institute of Multidisciplinary Research for Advanced Materials, Tohoku University, Sendai 980-8577, Japan

Email: iikubo@life.kyutech.ac.jp

Corresponding Author: Satoshi Iikubo

*E-mail: iikubo@life.kyutech.ac.jp   ***Postal address:** 2-4 Hibikino, Wakamatsu-ku, Kitakyushu-shi, Fukuoka, 808-0196, JAPAN

Author's E-mail address

K. Hirata: hirata-kenji@edu.life.kyutech.ac.jp

M. Koyama: koyama@mech.kyushu-u.ac.jp

K. Tsuzaki: tsuzaki.kaneaki.802@m.kyushu-u.ac.jp

H. Ohtani: h.ohtani@tagen.tohoku.ac.jp

Abstract

  The hydrogen diffusion behavior in BCC, FCC, and HCP iron has been investigated by means of first-principles calculations. Diffusion coefficients were estimated quantitatively from the migration energy derived by the Nudged elastic band method, and phonon calculations including the vibrations of all atoms at every stable and metastable site. Our calculations on the BCC structure show good agreement with those in the previous report. In the FCC structure as well, the calculated diffusion coefficients are in good agreement with experimental data. Our results suggest that the consideration of the antiferromagnetic state in FCC is important for the reproduction of experimental results. For the HCP structure, although there was a lack of systematic experimental results, our calculations predict that the diffusion coefficient is smaller than that in the case of the FCC sample. In the HCP lattice, there are two diffusion paths: one parallel to the c-axis and the other in the c-plane. The direction and the diffusion coefficient can be controlled by the tuning of c/a, which is the ratio of the lattice constants.

1. Introduction

Hydrogen is being increasingly used as a clean energy source that reduces the amount of carbon dioxide emitted into the atmosphere. Therefore, hydrogen-resistant structure materials have been sought for hydrogen-energy-related infrastructure. In this regard, steels are advantageous with respect to the strength and cost performance. Key factors affecting mechanical performance of steels under hydrogen environment are hydrogen content, distribution, and diffusivity. In particular, the diffusivity of hydrogen drastically alters fatigue properties which are the determinant factor for safety structure design. From a viewpoint of hydrogen diffusivity, close-packed structures are believed to show a low diffusivity of hydrogen, i.e. FCC and HCP structures. In steels, austenitic steels actually show a low diffusivity [1-3], which results in high resistance to fatigue crack growth in hydrogen environments [4].

On the other hand, there is few systematic knowledge about hydrogen diffusivity for another promising candidate, HCP structure. Because stable and single HCP phase cannot be obtained under ordinary pressure. Instead, deformation-induced HCP-martensitic transformation from austenitic phase was utilized to obtain high resistance to fatigue crack growth in Fe-Mn-Cr-Ni steel, which successfully endowed comparable fatigue crack growth resistance to stable austenitic steels [5]. Correspondingly, some indirect evidences of low diffusivity of HCP-martensite has been reported [6,7]. The utilization of HCP martensite is expected to give a new pathway for alloy design of hydrogen-resistant steels. However, because the effect of lattice defects including its interface on diffusivity cannot be quantified, experimental methodologies such as permeation test cannot determine underlying diffusivity along interstitial sites of HCP. Furthermore, the *c/a* and volume of HCP change sensitively by composition of alloys and constraint condition with parent phase. Thus, designing HCP-based hydrogen-resistant materials needs systematic and atomic-level insight revealed from the computational simulations.

From a theoretical point of view, the diffusion behavior of hydrogen has been studied using several simulation techniques [8-13]. First-principles calculations based on the density functional theory (DFT) have been used to determine the energetics associated with the migration of interstitial H atoms in crystalline metals. Since hydrogen is the lightest chemical element, its diffusion is affected by quantum mechanical effects. Quantum mechanical effects on the diffusion of interstitial atoms can be divided into two contributions. The first is due to the zero point energy (ZPE) of the ground state of a vibrating proton or, more generally, due to the presence of discrete vibrational energy levels and their occupied state at finite temperatures. The second contribution is due to quantum mechanical tunneling.

Kimizuka *et al*.[9] and Stefano *et al*.[10] have pointed out that it is difficult to explain the diffusivity of hydrogen with accuracy in BCC materials using the transition state theory (TST) since it cannot account for the quantum effect become prominent at low temperature. On the other hand, the diffusion coefficient calculated using the TST is in good agreement with experimental results for Ni and Ti that have the FCC and HCP closed packed structures, respectively[10,12]. This observation could be due to the quantum effect being negligible in those metals. Therefore, an investigation based on the TST in FCC and HCP irons would be insightful. Comparison of the hydrogen diffusivity in BCC, FCC, and HCP, missing piece of the study, make a significant contribution toward materials design for hydrogen-resistant steels.

In this study, we have investigated the hydrogen diffusion behavior in BCC, FCC, and HCP iron by means of first-principles calculations. Our calculation results for the BCC iron show good agreement with those of previous reports [9,10]. In the FCC iron, the calculated diffusion coefficients are compared with the experimental data. Our

70 calculations predict that the diffusion coefficient of the HCP sample which has several c/a is smaller than that of the

71 FCC sample. In the HCP lattice, there are two diffusion paths: one parallel to the c-axis and the other in the c-plane.

72 The direction and the diffusion coefficient can be controlled by the tuning of c/a, which is the ratio of the lattice

73 constants. The low and direction controllability of hydrogen diffusivity in HCP iron suggests a different paradigm in

74 steels under hydrogen environment.

2. Computational details

Following Wert and Zener [14] the interstitial diffusion coefficient is described as

$$D = nL^2\Gamma \quad (1)$$

where n is a numerical coefficient, whose value depends on the location of the interstitial positions, L and Γ are the jump distance projected onto the diffusion direction and the jump rate, respectively. In the Kehr approximation [15], the jump rate can be written as follows:

$$\Gamma = \frac{k_B T}{h} \exp(-\frac{\Delta E}{k_B T}) \quad (2)$$

where ΔE is the migration energy in the diffusion pathway. k_B, T and h indicate the Bolzmann constatnt, temperature and Planck constant, respectively. The simplest extension of this classical expression taking into account zero-point energy, the temperature-dependent part of the internal energy and the vibrational entropy is usually done by simply adding the difference in vibrational free energies, ΔG_{vib}, corresponding to the saddle point and the initial state, to the migration energy in the exponential term in Eq.(2). The corrected diffusivity is hence expressed as

$$D = nL^2 \frac{k_B T}{h} \exp(-\frac{\Delta E + \Delta G_{vib}}{k_B T}) \quad (3)$$

where

$$\Delta G_{vib} = G_{vib}^{saddle} - G_{vib}^{interstitial\ site} \quad (4).$$

The vibrational free energy G_{vib} in several states is explained as

$$G_{vib} = -k_B T \int_0^\infty g(\upsilon) \ln[2\sinh(\frac{h\upsilon}{2k_B T})] d\upsilon \quad (5)$$

where $g(\upsilon)$ is the phonon density of states and ν is vibrational frequency.

In order to calculate ΔE for hydrogen diffusion in iron, the climbing image nudged elastic band method[16] (CI-NEB) was used. The NEB method provides the means to find a minimum energy path (MEP) when the initial and final states of a process are known [17]. The CI-NEB method is an improved version of the NEB method, and it is used to locate the MEP and transition state for the diffusion of hydrogen in bulk Fe. We used the VTST code for the Vienna Ab initio Simulation Package (VASP) code [18,19] developed by Henkelman *et al*.[16]. The supercells of $Fe_{54}H$ ($3\times3\times3$), $Fe_{36}H$ ($2\times2\times2$), and $Fe_{96}H$ ($4\times4\times3$) were used for BCC, FCC, and HCP, respectively in the CI-NEB calculation. We set linear interpolation images between the initial and final states with three or five images, which were converged to the MEP with a $3\times3\times3$ mesh for k-point sampling in BCC and HCP. We used a $5\times5\times5$ mesh for k-point sampling with respect to FCC.

The lattice relaxation and total energy calculations were performed with the VASP code, which is based on DFT. The exchange and correlation functions were given by the generalized gradient approximation, as proposed by Perdew *et al*.[20]. We employed Blochl's projector-augmented wave (PAW) method as implemented by Kresse and Joubert [21, 22]. The Monkhorst-Pack method [23] is used to set the k-point mesh and a cutoff of 334.9 eV for the plane waves was applied. Before the NEB calculations were performed, structure optimizations were performed with a $13\times13\times13$ mesh for k-point sampling with a cutoff energy of 348.247 eV regarding BCC and FCC. In the calculation of HCP, we used a $15\times15\times9$ mesh for k-point sampling.

109   In this study, the magnetic properties were assumed to be ferromagnetic in BCC, antiferromagnetic in FCC, and

110   nonmagnetic in HCP samples. In the FCC iron, magnetic states have been investigated and it was suggested that the

111   antiferromagnetic state was stable [24-26]. However, the double-layered antiferromagnetic structure [25] causes the

112   lattice symmetry to change from cubic to tetragonal. Therefore, these two lattice types, namely, antiferromagnetic

113   FCC and antiferromagnetic FCT, were generated in the following manner. First, the lattice parameters were optimized

114   in the nonmagnetic FCC and HCP. The optimized lattice constants were $a = 3.44$ Å in FCC and $a = 2.46$ and $c = 3.89$

115   Å in HCP, respectively. These values are consistent with those reported in previous works[8,10,24,26]. The FCC

116   structure, which was optimized for the antiferromagnetic state, resulted in a tetragonal structure, which had $a = 3.46$

117   and $c = 3.75$ Å. The difference in the equilibrium volume between the antiferromagnetic FCT and nonmagnetic FCC

118   is estimated to be 10.3 %, which is expected to affect the diffusivity of hydrogen. Hence, we calculated the migration

119   energy of the antiferromagnetic FCT and FCC, which have the same equilibrium volume, by the NEB method. On

120   the other hand, although HCP has been calculated as antiferromagnetic state[26], the difference in the equilibrium

121   volume between the antiferromagnetic and nonmagnetic state was only 2.7%, which is comparatively lower than that

122   of FCC. Therefore, we have calculated the migration energy of hydrogen in the HCP in the nonmagnetic state since

123   the effect of the volume change is expected to be low.

124   Thermodynamic functions are obtained from phonon dispersions, which are calculated by the direct method [27]

125   with ab initio forces from VASP. To estimate the force due to displacement within the DFT calculation, we used the

126   plane wave energy cut off of 267.882eV, the convergence criterion for electric self-consistency loop of 10^{-6} eV, a Γ

127   point centered k-mesh of $2 \times 2 \times 2$, the Methefessel-Paxton smearing method with the width of the smearing in 0.2

128   eV, and a displacement of 0.01 Å.

129

130

131

132

133

134

135

136

137

138

139

140

141

142

143

144

145

146

3. Results and discussion

3.1. BCC
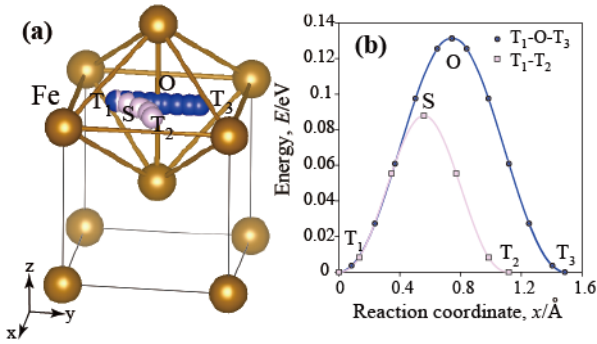
Fig.1. (a) The hydrogen migration pathways in BCC. O, T, and S represent the octahedral site, tetrahedral site, and saddle point, respectively. (b) The energy profiles for two paths: T_1-T_2 direct and T_1-O-T_3 indirect.

First, we have examined our calculated results for BCC and compared them with those reported in previous studies[8,10]. Figs.1 (a) and (b) show the migration pathways of the hydrogen atom in the BCC and the energy profiles for T_1-T_2 direct and T_1-O-T_3 indirect hopping, respectively. The minimum energy path along T_1-O-T_3 is almost straight, while along T_1-T_2 it seems to curve towards the O-site. This behavior is consistent with those reported in a previous paper[8]. From Fig.1(b), it is revealed that the T_1-T_2 direct hopping is a more stable transition path than T_1-O-T_3 indirect hopping. The "bare" migration energy ΔE can be estimated to be 0.088 eV. The calculated phonon dispersions of several states are given in Figs. 2. In fig.2(a), two branches at 29.6 and 43.7 THz correspond to the vibration of the hydrogen atom at tetrahedral interstitial site. The branches of hydrogen vibration derived from asymmetry of BCC lattice with hydrogen in T-site. The results have good agreement with the calculated values reported by Sakagami *et al.*[28]. From the Fig.2(b) we see that the hydrogen has one imaginary mode of vibrational frequency at the transition state of T_1-T_2. The imaginary mode means that there is dynamical instability at the site. The stable transition state for the diffusion has only one imaginary mode. Therefore, the S-site is a stable transition state. Furthermore, we estimated that the ΔZPE was 0.053 eV from these energy frequencies. The ZPE-corrected migration energy was 0.035 eV, which is in agreement with 0.042eV and 0.044eV presented in previous reports[8,10].
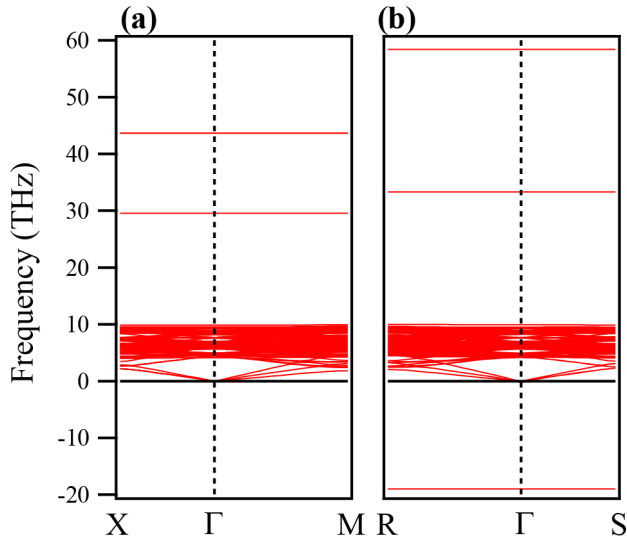
169

170 Fig. 2. The calculated phonon dispersions of a 56 atom-Fe supercell with hydrogen atom in (a) T-site and (b) the

171 saddle (S) point of T_1-T_2, respectively. The symmetry of the supercell describing the transition state is different

172 from that of the tetrahedral site, which is reflected in the labeling of the special points in the Brillouin zone.

173

174

175 **3.2. FCC**

176
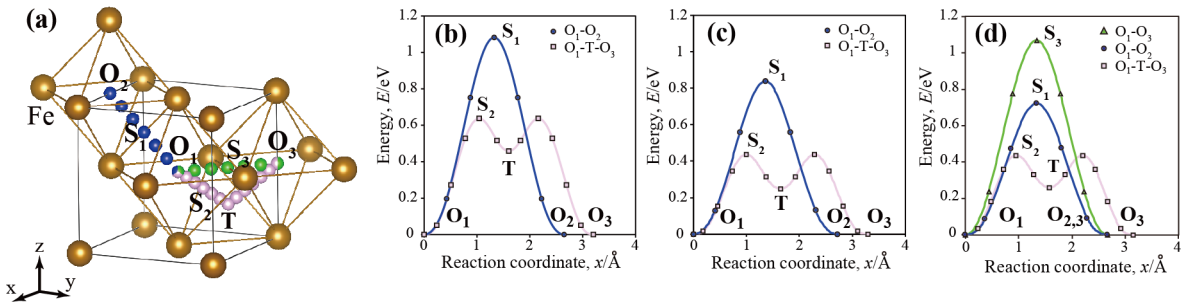
177

178 Fig.3. (a) The hydrogen migration pathways in FCC. (b) The energy profiles for O-T-O indirect and O-O direct paths

179 in nonmagnetic, (c) antiferromagnetic FCC, and (d) antiferromagnetic FCT, where the O_1-O_2, and O_1-O_3 paths are

180 distinguished.

181

182 Fig. 3(a) shows the migration pathways in the FCC and FCT lattices considered in this study. In the FCC case, the

183 stable interstitial site is the O-site, which is consistent with the result of Ismer *et al.*[11]. Three types of migration

184 pathways between the O-sites are indicated, namely, O_1-O_2 direct, O_1-T-O_3 indirect, and O_1-O_3 direct (which is

185 identical to the O_1-O_2 path in the case of FCC) paths. The energy profiles for these migration pathways in

186 nonmagnetic FCC, antiferromagnetic FCC, and antiferromagnetic FCT are shown Fig.3 (b)-(d). In antiferromagnetic

187 FCT, the two paths of the direct nearest neighbor O-sites are distinguished. In all cases, the energy barrier between

188 the nearest neighbor O-sites mediated by the T-site are lower than O_1-O_2 and O_1-O_3 direct hopping. Therefore, the

189 O_1-T-O_3 indirect migration pathway can be considered as a stable one. For antiferromagnetic FCT, there are two O-

7

T-O paths. One is in the same spin layer and another is the path between different spin layers. The more stable path is found in the same spin layer and the migration energies of all the diffusion pathways are listed in Table 1. The energy barrier of the antiferromagnetic FCC (0.44 eV) and FCT (0.44 eV) are consistent with the experimental migration energy, which was reported as 0.46 eV[29].

Figure 4 shows the phonon dispersion for each atomic configurations, (a) nonmagnetic FCC supercell with hydrogen in O-site and T-site, (b) saddle point, (c) antiferromagnetic FCC supercell with hydrogen in the interstitial sites in O-site and T-site, (d) saddle point, and (e) antiferromagnetic FCT. In Fig. 4(a), (c), and (e), several dispersionless mode mainly originated from the hydrogen vibration for different configurations are shown in the same figure, because the phonon dispersion derived from host Fe atoms is slightly changed. The hydrogen vibrations in an FCC Fe-25Cr-20Ni stainless steel alloy with a low hydrogen content has been reported by neutron spectroscopy [30]. The vibrational energy has been found to be ~ 130 meV(31 THz). This value has consistent with calculated vibrational energies of nonmagnetic FCC (139 meV), antiferromagnetic FCC (140 meV) and antiferromagnetic FCT (137 meV), respectively.

For the nonmagnetic FCC with hydrogen in O-site and T-site, there is no imaginary mode. Therefore we would like to point out that the T-site is not unstable, but a metastable site. On the other hand, the state with hydrogen in saddle point has one imaginary mode. Thus, the stable diffusion pathway of hydrogen is thought to be between the O-sites mediated by the T-sites in FCC. A similar behavior observed in antiferromagnetic FCC and FCT is shown in fig. 4 (c) ~ (e). From the figures, O-site and T-site are indicated as a stable interstitial site, and the saddle point between O_1-T in antiferromagnetic FCC and FCT have one imaginary mode and these states are revealed stable transition state of hydrogen diffusion. Ismer *et al*[11]. have reported similar results from first-principles calculations. Recently, Machida *et al.*[31] have deduced that the interstitial site for hydrogen in FCC is not only the O-site but also the T-site from neutron diffraction patterns under high pressure. Thus, our results are consistent with the calculated and experimental results.

Table 1 The calculated migration energy for hydrogen diffusion in nonmagnetic FCC, antiferromagnetic FCT and FCC, respectively.

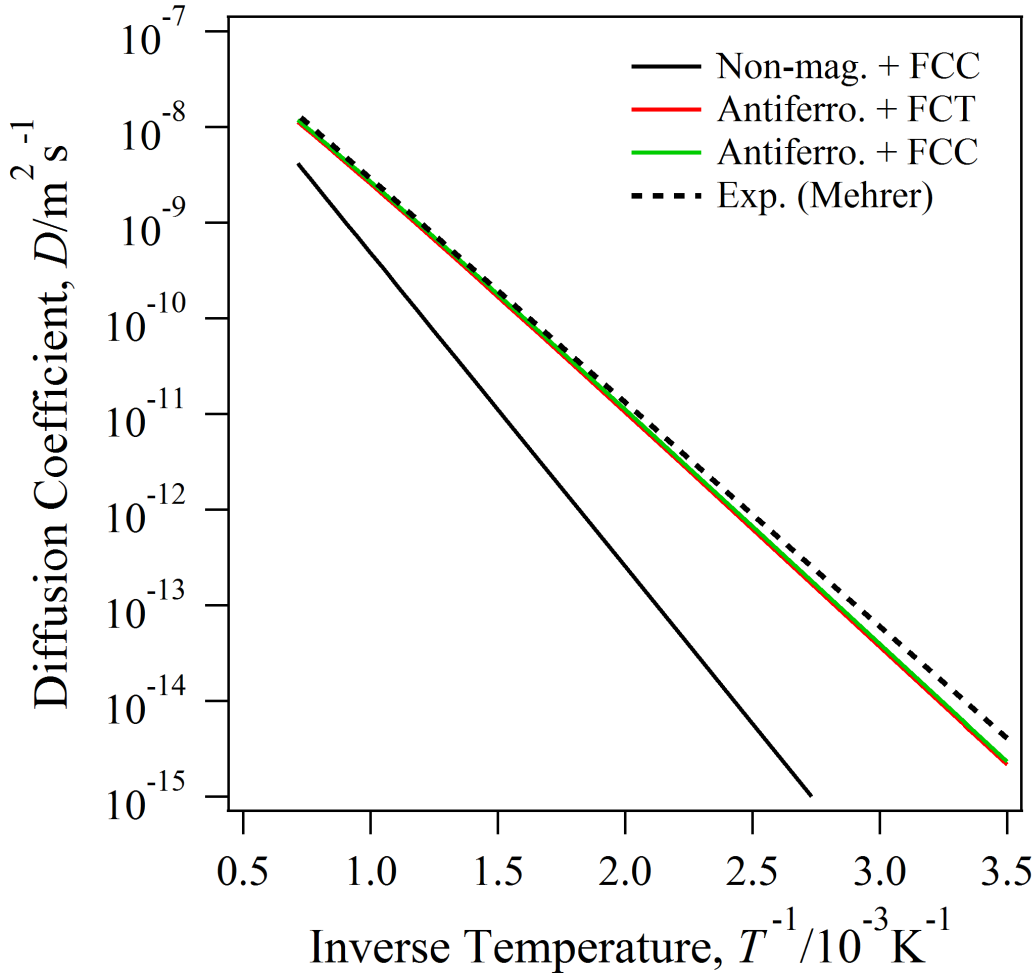|	Nonmagnetic FCC (eV)	Antiferromagnetic FCT (eV)	Antiferromagnetic FCC (eV)
O_1-T-O_3	0.64	0.44	0.44
O_1-O_3	1.08	1.07	0.84
O_1-O_2	-	0.72	-
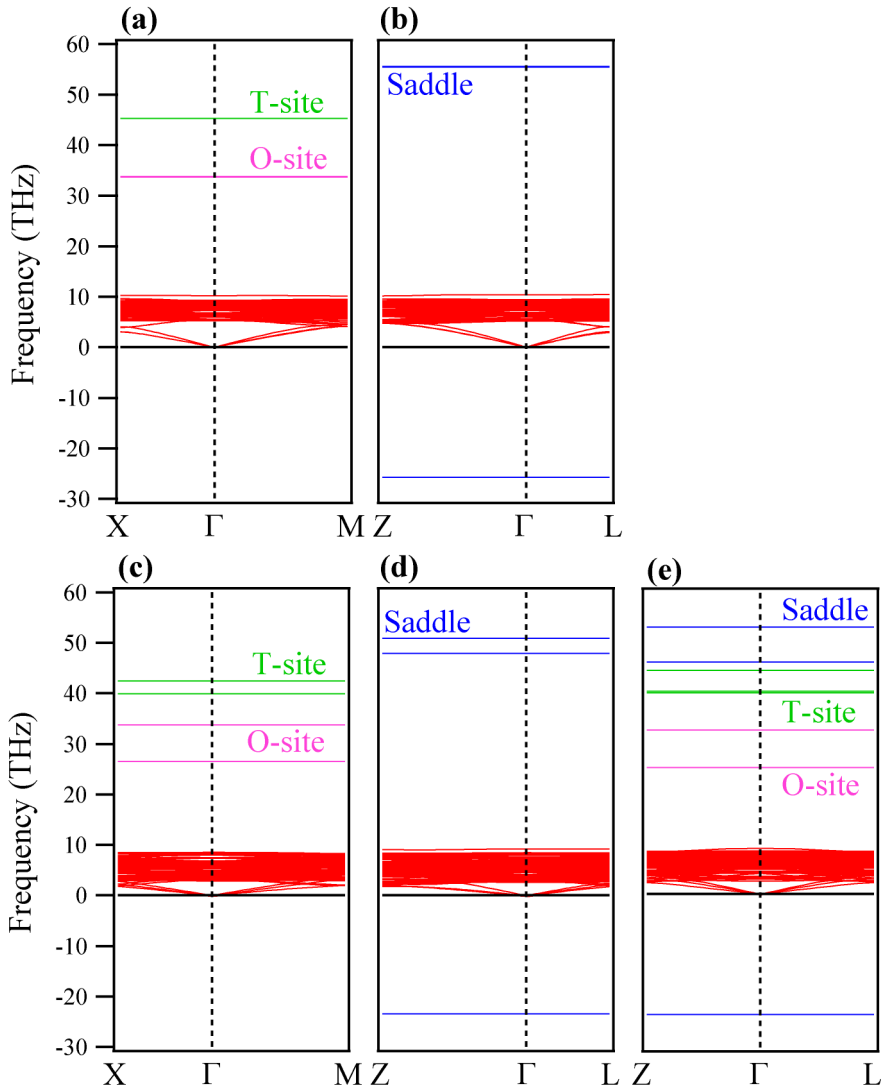
Fig. 4. The calculated phonon dispersions of a 32-atom Fe supercell with hydrogen atom in (a) O-site and T-site, and (b) saddle point in nonmagnetic FCC, respectively. The calculated phonon dispersions of antiferromagnetic FCC with hydrogen which states in (c) O-site and T-site, (d) saddle point, respectively. (e) the calculated phonon dispersions of antiferromagnetic FCT supercell with hydrogen which occupies several sites. The labeling of the special points in the Brillouin zone depends on the symmetry of several supercells. The pink, green and blue lines indicate the vibrational frequencies of hydrogen in O-site, T-site and saddle point, respectively.

Fig.5. The diffusion coefficient of hydrogen in FCC. The calculated values of nonmagnetic FCC, and antiferromagnetic FCT and FCC are denoted by the solid, red, and green lines, respectively. The dashed line indicates the experimental diffusion coefficient by Mehrer[29].

Diffusion coefficient of hydrogen between nearest stable O-site in FCC are described as

$$D_{FCC} = a^2 \Gamma \quad (6)$$

where a is a lattice constant. In this case, however, hydrogen diffusion occurs via metastable T-site. Therefore diffusion coefficient is modified as follows,

$$D'_{FCC} = \frac{1}{2} D_{FCC} (1 + 2\exp(-\frac{\Delta G_{\text{tet-oct}}}{k_B T}))^{-1} \quad (7).$$

$\Delta G_{\text{tet-oct}}$ is the difference of the free energy between hydrogen in tetrahedral and octahedral sites. Fig.5 shows an Arrhenius plot of the diffusion coefficient of hydrogen in nonmagnetic FCC, and antiferromagnetic FCC and FCT along with the experimental diffusion coefficient in pure FCC between 1183K (1000/T = 0.845) and 1373K (1000/T = 0.728) [29]. Our calculation results of the nonmagnetic state agree with those presented in a previous report[11]. The calculated diffusion coefficients of antiferromagnetic FCC and FCT are approximately same, and closely agree

10

with the experimental value for pure Fe. These results are consistent with a fact that the FCC has the antiferromagnetic

252 state as the ground state.

253

254

3.3. HCP

256

257
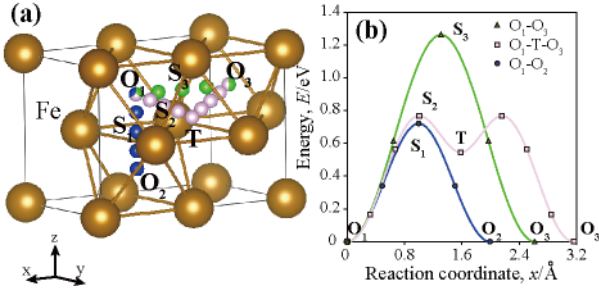
Fig.6. (a) The hydrogen migration pathways in HCP. (b) The energy profiles for several paths in the case of c/a = 1.58.

260

Fig. 6(a) shows the hydrogen atoms on migration pathways in the HCP iron. In this study, a fully relaxed lattice was obtained with c/a = 1.58. The migration energies of several diffusion paths are shown in Fig. 6(b). The stable interstitial site is found to be the O-site, while the T-site is metastable. The migration energies of O_1-O_2 direct, O_1-T-O_3 indirect, and O_1-O_3 direct hopping are estimated to be 0.72, 0.77, and 1.26, respectively. In case of c/a = 1.58, it is revealed that the O_1-O_2 direct diffusion path along the c-axis is slightly more stable than the diffusion path via the T-site on c-plane.

The calculated phonon dispersion of nonmagnetic HCP supercell with hydrogen in O-site and T-site is shown in Fig. 7 (a). Fig. 7 (b) and (c) show the calculated phonon dispersions of the saddle points S_1 between O_1-O_2 and S_2 between O_1-T. The hydrogen vibrational energy of dhcp FeH has been reported as 103meV by inelastic neutron scattering spectrum [32] and calculated value (140 meV, 110meV) with hydrogen in O-site is slightly higher than the experimental value. The difference of vibrational energy between experimental and calculated values can be caused by the difference of the metal-hydrogen distance.

For the state with hydrogen in O-site and T-site, there no imaginary mode. Therefore, these interstitial sites are stable from the view point of dynamics. On the other hand, the two states of saddle point have one imaginary mode derived from hydrogen. Therefore, both the O_1-O_2 path along the c-axis and the O_1-T-O_3 path in the c-plane can serve as stable diffusion paths in HCP.

277

278
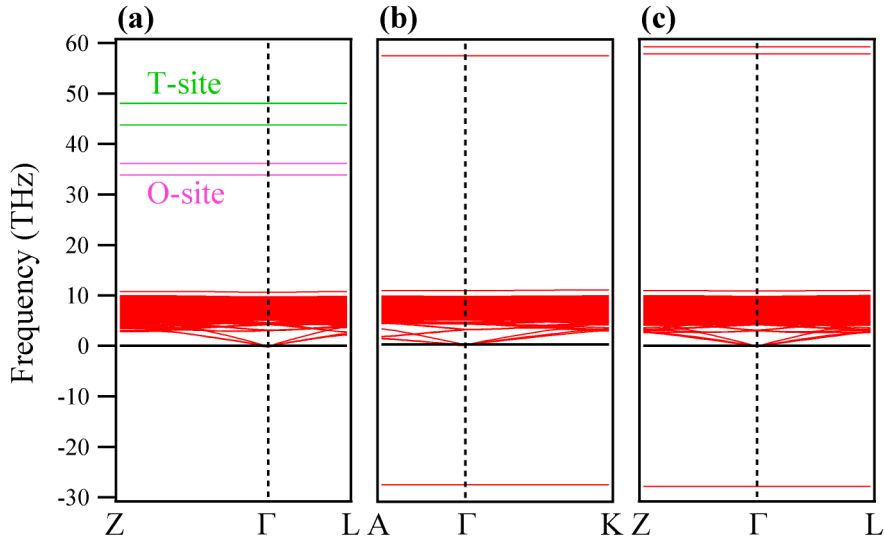
Fig. 7. The calculated phonon dispersions of a 96-atom Fe supercell with hydrogen atom in (a) O-site and T-site, (b) the saddle point of S_1 between O_1-O_2 and (c) S_2 between O_1-T in nonmagnetic HCP, respectively. The labeling of the special points in the Brillouin zone depends on the symmetry of several supercells. The pink and green lines indicate the vibrational frequencies of hydrogen in O-site and T-site, respectively.
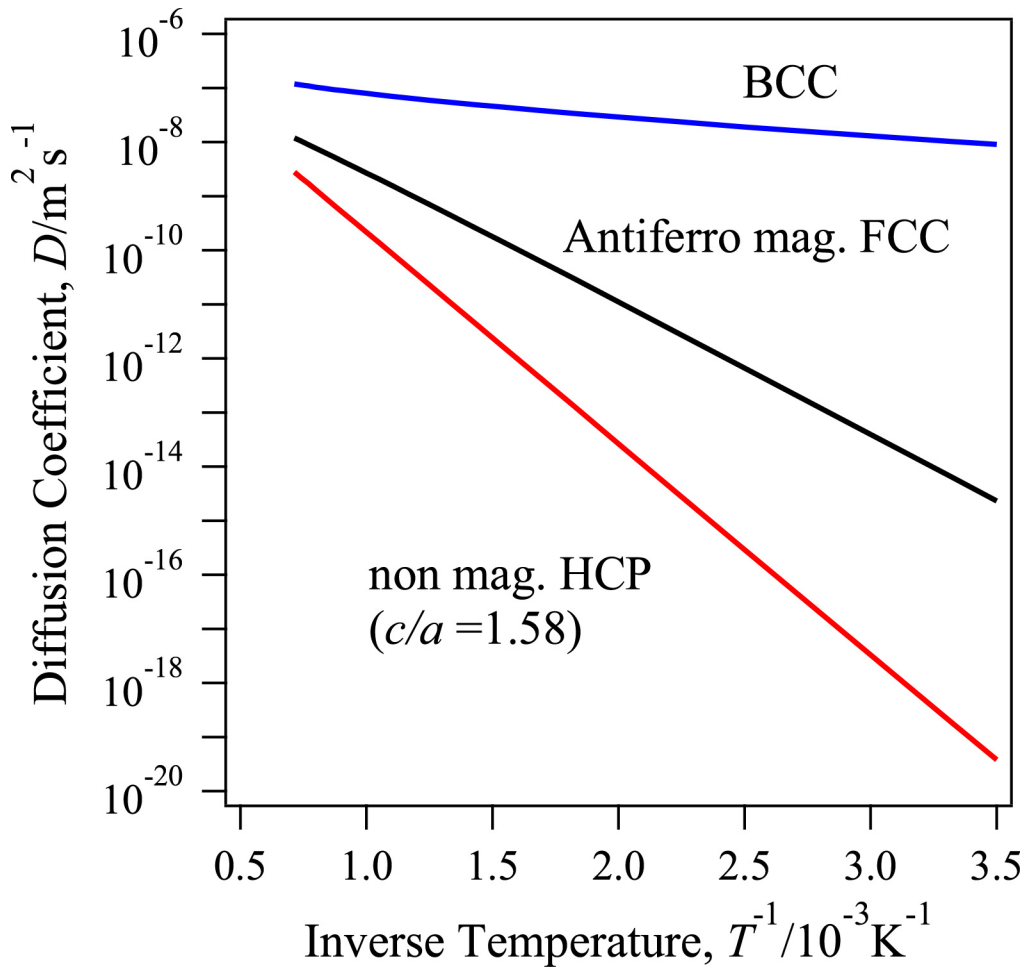
Fig.8 The Arrhenius plot of the diffusion coefficient of hydrogen in HCP and antiferromagnetic FCC. The red solid line indicates the diffusion coefficient for HCP with $c/a = 1.58$. The black and blue lines indicate the diffusion coefficient for antiferromagnetic FCC and BCC, respectively.

Here the diffusion coefficient in BCC, FCC, and HCP are compared. Although the hydrogen diffusion in BCC is isotropic, that in HCP is anisotropic along c-axis. Therefore, hydrogen diffusion in HCP must be considered with a coordination number between nearest stable O-site along c-axis. The diffusion coefficient in BCC and HCP are described as follows, respectively.

$$D_{BCC} = \frac{1}{12}a^2\Gamma \quad (8)$$

$$D_{HCP} = \frac{1}{4}c^2\Gamma \quad (9)$$

Fig.8 shows an Arrhenius plot of the diffusion coefficient of hydrogen in HCP for $c/a = 1.58$, along with relevant data of the antiferromagnetic FCC and BCC. The diffusion coefficient for HCP is revealed to be lower than that for FCC and BCC. Hence, materials that have the HCP structure can be considered to have the potential for resistance against hydrogen embrittlement that could either equal or even surpass FCC materials. This result has qualitatively agreement with the experimental result: the hydrogen diffusion behavior has not been changed on epsilon martensitic

13

304   transformation, which is the transformation from FCC to HCP, by Koyama *et al.* [6, 7]. On the other hand, c/a of

305   FeMn steels with epsilon martensite was reported to be 1.63 from experiments[33]. The different c/a values obtained

306   from different experiments are assumed to be due to the additive elements present in the alloy. Therefore, we have

307   investigated the c/a and volume dependence of hydrogen diffusivity in HCP because these values are expected to be

308   influenced by additive elements in actual materials.

309

310
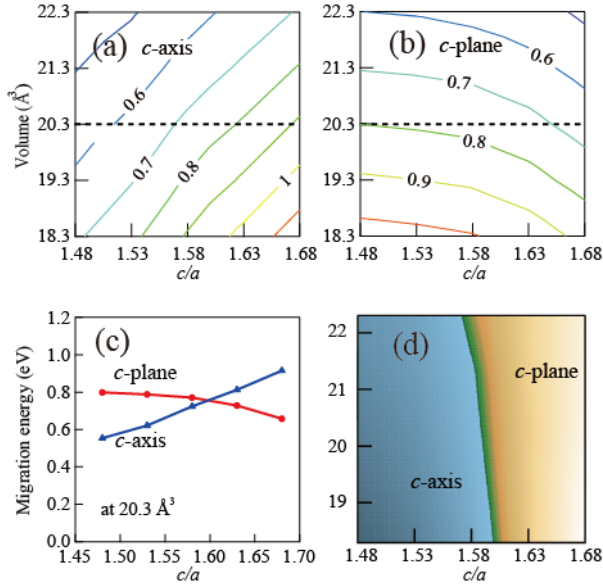
311

312   Fig.9. The migration energy in eV of (a) O_1-O_2 along c-axis and (b) O_1-T-O_3 on the c-plane with respect to volume

313   and c/a of HCP. (c) Comparison of the hydrogen migration energies along c-axis and on the c-plane on the cross-

314   section, denoted by dashed line in (a) and (b). (d) The difference of migration energy between c-axis and c-plane.

315   The left and right sides indicates c-axis and c-plane diffusion dominated region, respectively.

316

317   From the calculated energy profiles, we found an interesting behavior of hydrogen in HCP iron. This was the

318   anisotropic diffusion of hydrogen depending on c/a. Fig.9 shows the relationship between the migration energy,

319   volume, and c/a of HCP. The migration energies of O_1-O_2 along the c-axis and O_1-T-O_3 on the c-plane are indicated

320   in Fig.9(a) and (b), respectively. The equilibrium volume and c/a of nonmagnetic HCP are 20.3 Å^3 and 1.58,

321   respectively. The level lines of migration energy of O_1-O_2 are at about 45° and are assumed to be affected equally by

322   a change in volume and c/a ratio. On the other hand, the lines of migration energy of O_1-T-O_3 seem to shift slightly

323   with changing c/a ratio and hence they are considered to be affected to a lower extent by the change in c/a.

324   The c/a-dependent migration energies of both the pathways are shown in Fig.9(c). The data corresponds to the cross-

325   section marked using dashed lines in Fig.9(a) and (b). The diffusion pathway in the c-plane becomes stable with

326   increasing c/a values whereas the path along the c-axis becomes unstable. The stable pathways are found to be along

327   the c-axis below $c/a \sim 1.6$ and in the c-plane above $c/a \sim 1.6$. Fig. 9(d) indicates the stable pathways with respect to

328   volume and c/a. The blue and orange regions indicate which is the stable diffusion paths. It is revealed that the stable

329   diffusion path is along the c-axis O_1-O_2 below $c/a \sim 1.6$ and the c-plane O_1-T-O_3 becomes stable above $c/a \sim 1.6$.
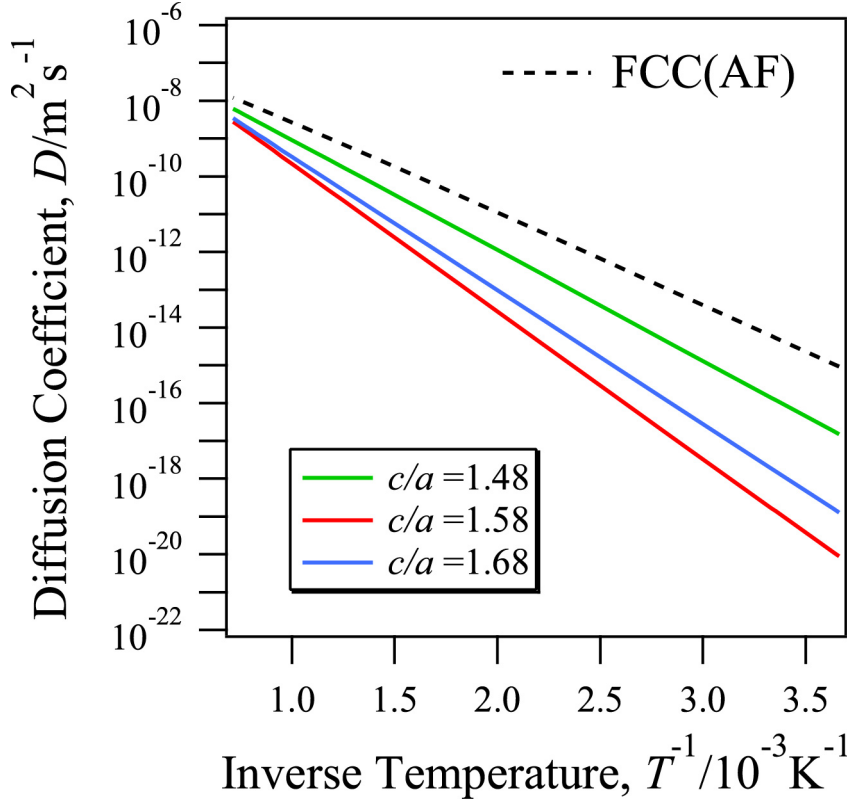
Fig.10. The Arrhenius plot of the diffusion coefficient of hydrogen in HCP with c/a = 1.48, 1.58, and 1.68, respectively. Dashed line indicates the calculated results of antiferromagnetic FCC.

From the migration energies investigated above, the diffusion coefficient was estimated in the range of c/a= 1.48–1.68. For the calculation of diffusion coefficient in the case of c/a = 1.68, the diffusion path contains the metastable T-site. Therefore diffusion coefficient is modified as follows,

$$D'_{HCP} = \frac{3}{2} D_{c-plane} (1 + 2\exp(-\frac{\Delta G_{tet\text{-}oct}}{k_B T}))^{-1} \quad (10)$$

where

$$D_{c-plane} = \frac{3}{2} a^2 \Gamma \quad (11).$$

The equation (11) was developed by considering a coordination number between stable O-sites in c-plane. The Arrhenius plots of the diffusion coefficient of hydrogen in HCP at 20.3 Å^3 are given in Fig.10. Minimum diffusivity is observed around $c/a \sim 1.6$, and the diffusion coefficient increases with both increasing and decreasing c/a ratio. However, the direction of the H diffusion changes with the value of c/a. When c/a is higher than ~1.6, the diffusion path is in the c-plane O_1-T-O_3. On the other hand, when c/a is lower than ~1.6, the diffusion path is along the c-axis. Recently, the diffusion coefficient of hydrogen in HCP has been reported by theoretical calculation for $c/a \sim 1.58$ [13]. On the other hand, actual experimental c/a in FeMn steels was estimated at ~ 1.63[33]. Our findings regarding the diffusivity in the HCP lattice has important implications in terms of the possibility of control over the magnitude

15

350 and direction of the diffusion behavior. By tuning the *c/a* ratio, which can be performed by adding some elements

351 into the iron, the magnitude and direction of the H diffusion can be controlled independently in the range *c/a* < 1.6

352 or *c/a* > 1/6. For example, the *c/a* ratio of HCP-Fe can be changed by loading high pressure [34] and addition of

353 alloying elements [35]. In fact, the change with respect to the *c/a* ratio of HCP-Co bulk and film has been reported

354 by these methods[36,37]. This diffusion characteristic, which is a general physical property of the HCP lattice, can

355 now be used to produce a new functionality of the HCP alloy system.

356

357

358

359

360

361 ## 4. Conclusion

362 Hydrogen diffusivity in HCP iron, which is the promising candidate for high resistance to fatigue crack growth has

363 been investigated by a theoretical calculation and compared to those of BCC and FCC. In BCC and FCC iron, the

364 calculated results with respect to stable interstitial sites are in good agreement with those reported in previous

365 experimental and theoretical investigations. In the FCC case, the stable diffusion path is between the O-sites mediated

366 by the T-site. The calculated hydrogen diffusion coefficient was enhanced and agreed with experimental results,

367 when the antiferromagnetic state was considered. In HCP, the interstitial site was found to be the O-site and the

368 migration energy for the hydrogen diffusion was estimated to be higher than that in FCC, which causes low diffusivity

369 of H in the HCP lattice. The hydrogen diffusion was seen to have an anisotropic behavior that depended on the *c/a*

370 ratio. At an equilibrium volume of nonmagnetic HCP, the stable pathways were found to be the direct O-site path

371 along the *c*-axis when *c/a* < 1.6 and the path between the O-sites mediated by the T-site on the *c*-plane when *c/a* >

372 1.6. The diffusion coefficient of hydrogen in HCP was found to be lower than that in FCC and it can be concluded

373 that the epsilon martensite has a low susceptibility to hydrogen embrittlement. The low and direction controllability

374 of hydrogen diffusivity in HCP iron suggests a different paradigm in steels under hydrogen environment.

375

376

381

382

383

16

References

384

385 [1] T.P. Perng and C.J. Alstetter: *Metall. Trans. A*, 1987, vol. 18, pp. 123-134.

386 [2] T. Kanezaki, C. Narazaki, Y. Mine, S. Matsuoka and Y. Murakami: *Int. J. Hydrogen Energ.*, 2008, vol. 33, pp.

387 2604-2619.

388 [3] M. Koyama, E. Akiyama, K. Tsuzaki and D. Raabe: *Act. Mater.*, 2013, vol. 61, pp. 4607-4618.

389 [4] P. Sofronis: *J. Mech. Phys. Solids.*, 1995, vol. 43, pp. 1385-1407.

390 [5] K. Tsuzaki, K. Fukuda, M. Koyama and H. Matsunaga: *Scr. Mater.*, 2016, vol. 113, pp. 6-9.

391 [6] M. Koyama and K. Tsuzaki: *ISIJ Int.*, 2015, vol. 55, pp. 2269-2271.

392 [7] M. Koyama, Y. Abe, K. Saito, E. Akiyama, K. Takai and K. Tsuzaki: *Scr. Mater.*, 2016, vol. 122, pp. 50-53.

393 [8] D. E. Jiang and E. A. Carter: *Phys. Rev. B*, 2004, vol. 70, p. 064102.

394 [9] H. Kimizuka, H. Mori and S. Shigenobu: *Phys. Rev. B*, 2011, vol. 83, p. 094110.

395 [10] D. D. Stefano, M. Mrovec and C. Elsässer: *Phys. Rev. B*, 2015, vol. 92, p. 224301.

396 [11] L. Ismer, T. Hickel and J. Neugebauer: *Phys. Rev. B*, 2010, vol. 81, p. 094111.

397 [12] A.V. Bakulin, T.I. Spiridonova, S.E. Kulkova, S. Hocker and S. Schmauder: *Int. J. Hydrogen Energ.*, 2016, vol.

398 41, pp. 9108-9116.

399 [13] Y. He, Y. Li, C. Chen and H. Yu: *Int. J. Hydrogen Energ.*, 2017, vol. 42, pp. 27438-27445.

400 [14] C. Wert and C. Zener: *Phys. Rev.*, 1949, vol. 76, pp. 1169-1175.

401 [15] K.W. Kehr: *Theory of the Diffusion of Hydrogen in Metals*, in: G. Alefeld, J. Völkl (Eds.), Hydrogen in Metals

402 I, Springer, Berlin, Heidelberg, 1978, pp. 197-226.

403 [16] G. Henkelman, B.P. Uberuaga and H. Jónsson: *J. Chem. Phys.*, 2000, vol. 113, p. 9901.

404 [17] H. Jónsson, G. Mills and K. W. Jacobsen: in: B. J. Berne, G. Ciccotti, D. F. Coker (Eds.), Nudged elastic band

405 method for finding minimum energy paths of transitions, Classical and Quantum Dynamics in Condensed Phase

406 Simulations, World Scientific, Singapore, 1998, pp. 385-404.

407 [18] G. Kresse and J. Furthmüäller: *Phys. Rev. B*, 1996, vol. 54, p. 11169.

408 [19] G. Kresse and J. Furthmüäller: *Comp. Mater. Sci.*, 1996, vol. 6, p. 15.

409 [20] J. P. Perdew, K. Burke and M. Ernzerhof: *Phys. Rev. Lett.*, 1997, vol. 78, p. 1396.

410   [21] P. E. Blöchl: *Phys. Rev. B*, 1994, vol. 50, p. 17953.

411   [22] G. Kresse and D. Joubert: *Phys. Rev. B*, 1999, vol. 59, p. 1758.

412   [23] H.J. Monkhorst and J.D. Pack: *Phys. Rev. B*, 1976, vol. 13, p. 5188.

413   [24] H. C. Herper, E. Hoffmann and P. Entel: *Phys. Rev. B*, 1999, vol. 60, p. 3839.

414   [25] D. E. Jiang and E. A. Carter: *Phys. Rev. B, 2003*, vol. 67, p. 214103.

415   [26] Z. Lu, W. Zhu, T. Lu and W. Wang: *Modelling Simul. Mater. Sci. Eng.*, 2014, vol. 22, p. 025007.

416   [27] K. Parlinski, Z.Q. Li and Y. Kawazoe: *Phys Rev Lett.*, 1997, vol. 78, pp. 4063-4066.

417   [28] Y. Sakagami, R. Matsumoto, D. Alfè, D. Taketomi, T. Enomoto and N. Miyazaki: *Trans. Mater. Res. Soc. Jpn.*,
418   2012, vol. 37, pp. 1–6.

419   [29] H. Mehrer ed.: *Diffusion in solid Metals and Alloys*, Landolt-Börnstein New Series, Group Ⅲ, 69, Springer,
420   1990, p. 529.

421   [30] S.A. Danilkin, D. Delafosse, H. Fuess, V.G. Gavriljuk, A. Ivanov, T. Magnin and H.Wipf: *Appl. Phys. A (Suppl.)*,
422   vol. 74, pp. 992–994.

423   [31] A. Machida, H. Saitoh, H. Sugimoto, T. Hattori, A. Sano-Furukawa, N. Endo, Y. Katayama, R. Iizuka, T. Sato,
424   M. Matsuo, S. Orimo and K. Aoki: *Nat. Commun.*, 2014, vol. 5, p. 5063.

425   [32] K. Cornell, H. Wipf, V.E. Antonov, T.E. Antonova, A.I. Kolesnikov, E.G. Ponyatovsky and B. Dorner: *Pol. J.*
426   *Chem.*, 1997, vol. 71, pp. 1792-1796.

427   [33] D. T. Pierce, J. A. Jiménez, J. Bentley, D. Raabe, C. Oskay and J. E. Witting: *Act. Mater.*, 2014. vol 68, pp. 238-
428   253.

429   [34] C. M. S. Gannarelli, D. Alfè and M. J. Gillan: *Phys. Earth Planet. Inter.*, 2005, vol. 152, pp. 67-77.

430   [35] T. Sakai, E. Ohtani, N. Hirao and Y. Ohishi: *Geophys. Res. Lett.*, 2011, vol. 38, p. L09302.

431   [36] D. Antonangeli, L.R. Benedetti, D.L. Farber, G. Steinle-Neumann, A.L. Auzende, J. Badro, M. Hanfland and
432   M. Krinch: *Appl. Phys. Lett.*, 2008, vol. 92, p. 111911.

433   [37] S. Hinata, R. Yanagisawa, S. Saito and M. Takahashi: *J. Appl. Phys.*, 2009, vol. 105, p. 07B718.

434

435

436

437

438

19

494

495 Table 1 The calculated migration energy for hydrogen diffusion in nonmagnetic FCC, antiferromagnetic FCT and

496 FCC, respectively.

497

	Nonmagnetic FCC (eV)	Antiferromagnetic FCT (eV)	Antiferromagnetic FCC (eV)
O_1-T-O_3	0.64	0.44	0.44
O_1-O_3	1.08	1.07	0.84
O_1-O_2	-	0.72	-